Supplementary Information

Unexpected tautomeric equilibria of the carbanion-enamine intermediate in pyruvate oxidase highlight unrecognized chemical versatility of thiamin

Danilo Meyer[1#], Piotr Neumann[2#], Eline Koers[1], Hanno Sjuts[1], Stefan Lüdtke[1], George M. Sheldrick[3], Ralf Ficner[2], and Kai Tittmann[1,*]

[1]Albrecht-von-Haller Institute & Göttingen Center for Molecular Biosciences, Georg-August University Göttingen, D-37077 Göttingen, Germany, [2]Institute for Microbiology and Genetics, Georg-August University Göttingen, [3]Institute of Inorganic Chemistry, Georg-August University Göttingen

[#] Both authors contributed equally to this study.

* To whom correspondence should be addressed:
K.T.: phone: +49-551-3914430, fax: +49-551-395749, E-mail: ktittma@gwdg.de

SI Methods

Crystallization and X-ray crystallographic analysis

Recombinantly expressed pyruvate oxidase from *Lactobacillus plantarum* was crystallized by the hanging-drop vapor-diffusion method and using ammonium sulfate as precipitant (1). Crystals were soaked for 30-60 s in reservoir solution containing 100 mM pyruvate and 25% (*v*/*v*) glycerol, and were subsequently flash-cooled by direct immersion into liquid nitrogen. After complete consumption of physically dissolved substrate oxygen due to enzyme-catalyzed turnover, the yellowish protein crystals became colorless indicating that the bound flavin cofactor had been fully reduced. Since the ThDP and FAD cofactors operate unsynchronized in pyruvate oxidase, pyruvate is still bound and decarboxylated by ThDP (1, 2). Electron transfer from the ThDP post-decarboxylation carbanion-enamine intermediate to the fully reduced FAD, however, is blocked, hence the catalytic cycle stalls at this state and the hydroxyethyl-ThDP carbanion-enamine accumulates to full occupancy driven by quasi-irreversible decarboxylation of the pyruvate-ThDP adduct (2-lactyl-ThDP).

Two complete data sets from two individual crystals were collected at ESRF beamline 14.4 at 100 K in Grenoble, France. In order to minimize radiation damage, we collected for each crystal several partial data sets (coverage ~40°) with overlapping angular range at different spots of the crystal (separated by a distance of at least two times the beam size), and merged only these parts having no signs of detectable radiation damage as evidenced by low Rmerge (analysis of Rmerge vs batch plot). Data were processed and scaled with XDS (3). The previously determined structure of pyruvate oxidase variant Phe479Trp in complex with the carbanion-enamine intermediate (pdb code 2EZT) (1), solved at a resolution of 2.29 Å, was used as a starting model for initial rigid-body refinements. Further iterative cycles of model building and refinement were carried out using COOT (4), PHENIX (5) and finally Shelx-97 (6) until the free R-factor and the crystallographic R-factor had converged. All non-

hydrogen atoms were refined with anisotropic displacement parameters. Hydrogens of the protein were added by the Shelx-implemented "riding model" for final refinement cycles. Both bulk solvent correction and anisotropic scaling have been applied. Initially applied in-plane restraints for the suspected aromatic thiazolium and aminopyrimidine rings of the ThDP cofactor were gradually relaxed in late stages of refinement until the model was in good agreement with the electron density maps. The two structures were refined using Shelx-97 to an R_{work}/R_{free} of either 8.83%/11.17% (Fo > 4σ; crystal A) or 9.77%/12.26% (Fo > 4σ, crystal B) against data up to 1.09 (A) and 1.13 Å (B) resolution (SI Table 1). Estimation of bond-length and bond angle esd's was carried out by full-matrix refinement using a pre-release version of Shelx-11. In total, >135.000 parameters were simultaneously fitted.

The final models consist of residues 9-591 (out of 603) for each of the two monomers, 2 hydroxyethyl-ThDP carbanion-enamine intermediates, 2 two-electron reduced FAD cofactors, 2 Mg^{2+} ions, 4 pyruvate molecules, 2 phosphates, and solvent molecules (SI Table 1).

Stopped-flow kinetics

The reductive half-reaction of POX with artificial substrate acetaldehyde was analyzed by stopped-flow kinetics as recently described (7). 2 mg/ml POX was reacted with different concentrations of acetaldehyde or d_1-acetaldehyde under anaerobic conditions in 0.2 M potassium phosphate buffer, pH 6.0 in 1+1 mixing ratio at 25 °C. Reaction was monitored at 457 nm (intrinsic FAD absorbance). Microscopic rate constants of turnover were estimated by global fit analysis using program Dynafit (8).

Reactivity of reduced POX containing the HEThDP carbanion-enamine and the two-electron reduced FAD was analyzed by stopped-flow kinetics. 12 mg/ml POX (HEThDP carbanion-enamine/$FADH^-$) in anaerobic 0.2 M potassium phosphate buffer, pH 6.0 was reacted with 50 mM pyruvate in air-saturated, 0.2 M potassium phosphate buffer, pH 6.0 in 1+10 mixing ratio at 25 °C.

References SI Methods

1. Wille G, *et al.* (2006) The catalytic cycle of a thiamin diphosphate enzyme examined by cryocrystallography. *Nat Chem Biol* 2: 324-328.
2. Tittmann K, *et al.* (2003) NMR analysis of covalent intermediates in thiamin diphosphate enzymes. *Biochemistry* 42: 7885-7891.
3. Kabsch W (1993) Automatic Processing of Rotation Diffraction Data from Crystals of Initially Unknown Symmetry and Cell Constants. *J Appl Crystallogr* 26:795-800.
4. Emsley P & Cowtan K (2004) Coot: model-building tools for molecular graphics. *Acta Crystallogr Sect D: Biol Crystallogr* 60:2126-2132.
5. Adams PD, *et al.* (2002) PHENIX: building new software for automated crystallographic structure determination. *Acta Crystallogr Sect D: Biol Crystallogr* 58:1948-1954.
6. Sheldrick GM (2008) A short history of SHELX. *Acta Crystallogr Sect A* 64:112-122.
7. Tittmann K, *et al.* (2000) Mechanism of elementary catalytic steps of pyruvate oxidase from Lactobacillus plantarum. *Biochemistry* 39:10747-54.
8. Kuzmic P (1996) Program DYNAFIT for the analysis of enzyme kinetic data: application to HIV proteinase. *Anal Biochem* 237: 260-273.

SI Tables, Figures and Schemes

Supp. Table 1: Crystallographic data statistics

Crystal	***Lp*POX wild-type with HEThDP carbanion-enamine and two-electron reduced FAD**	
Data collection	**Crystal A**	**Crystal B**
Space group	C 2 2 2_1	C 2 2 2_1
a, b, c (Å)	118.60, 154.40, 165.42	119.07, 154.46, 165.82
α, β, γ (°)	90.00, 90.00, 90.00	90.00, 90.00, 90.00
Wavelength (Å)	0.9	0.9
X-ray source	Beamline 14.4, ESRF (Grenoble)	Beamline 14.4, ESRF (Grenoble)
Resolution range (Å)	44.69-1.09 (1.16-1.09)	47.69-1.13 (1.16-1.13)
No. of unique reflections	611332 (106460)	549376 (38989)
Completeness	98.1 (94.9)	97.5 (93.9)
R_{merge} (%)	6.7 (52.4)	9.4 (50.4)
Average I/σ(I)	12.05 (2.17)	7.33 (2.2)
Redundancy	3.9 (2.9)	2.9 (2.3)
Refinement		
Resolution (Å)	44.69-1.09	41.07-1.13
Monomers per AU	2	2
No. of atoms / Average B-factors (Å^2)	12091 / 13.9	11721 / 12.9
Protein	9737 / 9.8	9612 / 9.3
Ligands overall	254 / 11.0	236 / 11.9
TDM (carbanion-enamine)	58/6.7	58/6.9
FAD (two-electron reduced)	106/6.0	106/5.4
Waters	2100 / 33.2	1873 / 31.2
R_{work} (%) Fo > 4 sig (Fo) / all data	8.83 / 11.88	9.77 / 12.25
R_{free} (%) Fo > 4 sig (Fo) / all data	11.17 / 14.24	12.26 / 14.94
Figure of merit	0.98	0.98
GooF	1.634	1.635
RMS deviations		
Bond lengths (Å)	0.015	0.014
Angles (°)	2.142	2.051
Specific comments	Hydrogens assignable for carbanion-enamine	Hydrogens assignable for reduced FAD
pdb code	4FEG	4FEE

Values in parentheses indicate the specific values in the particular highest resolution shell. $R_{merge} = \Sigma_{hkl}\Sigma_i|I_i(hkl) - \langle I_i(hkl)\rangle|/ \Sigma_{hkl}\Sigma_i I_i\langle(hkl)\rangle$, where the sum i is over all separate measurements of the unique reflection hkl. $R_{work} = \Sigma_{hkl}||F_{obs}|-|F_{calc}||/\Sigma_{hkl}|F_{obs}|$. R_{free} was calculated as R_{work}, but summed over a 2 % test set of randomly selected reflections.

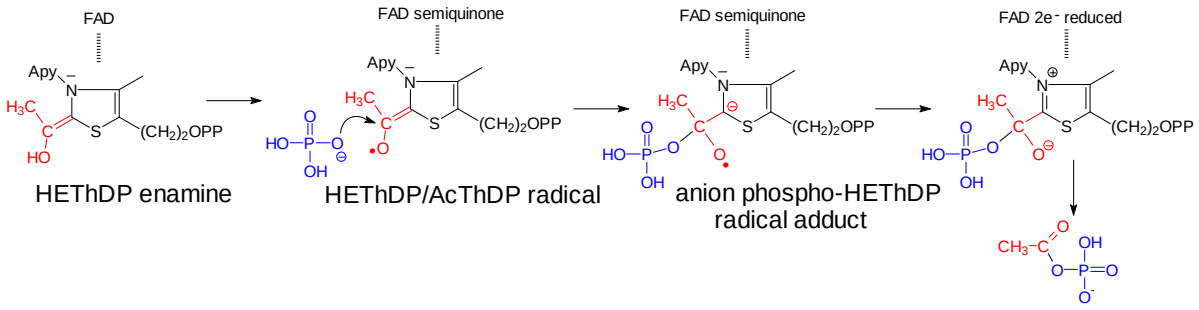

SI Fig. 1. Proposed mechanism of redox-coupled acyl transfer to phosphate catalyzed by POX from *Lactobacillus plantarum* (1).

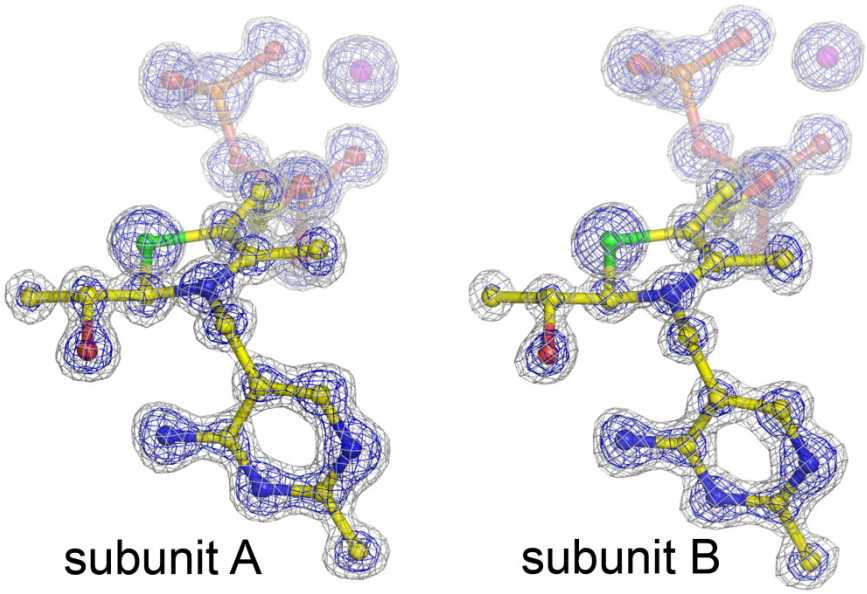

SI Fig. 2. Structure of the hydroxyethyl-ThDP carbanion-enamine intermediate in the two active sites of pyruvate oxidase are exemplified shown for crystal B (the asymmetric unit contains a nonfunctional dimer with two active sites). The final refined model of the intermediate in ball-and-stick representation and the corresponding 2mFo-DFc electron density map contoured at 4σ (blue) and 2σ (grey) are shown.

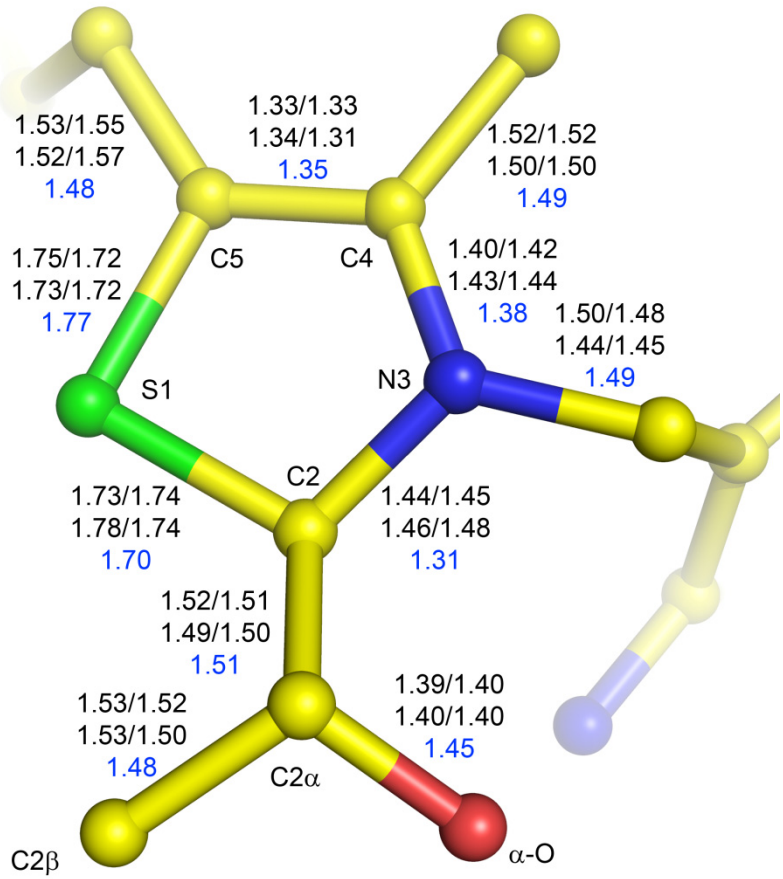

SI Fig. 3. Bond lengths of the thiazolium ring of the carbanion-enamine intermediate in POX in comparison to these of nonenzymic 2α-hydroxyethyl-thiamin diphosphate (2). First line of labels: crystal A subunit A/subunit B, second line: crystal B subunit A/subunit B, third line: nonenzymic 2α-hydroxyethyl-thiamin diphosphate. The bond-length esd's of the enzyme intermediate vary between 0.01 and 0.02 Å as estimated by full-matrix refinement using a pre-release version of Shelx-2011. Note that bonds C2-N3 and C2-S1 are markedly longer than expected for a fully aromatic thiazolium, whereas bond C2α-O is shorter compared to the nonenzymic compound. Refinement of the carbanion-enamine intermediate in POX was carried out without any restraint.

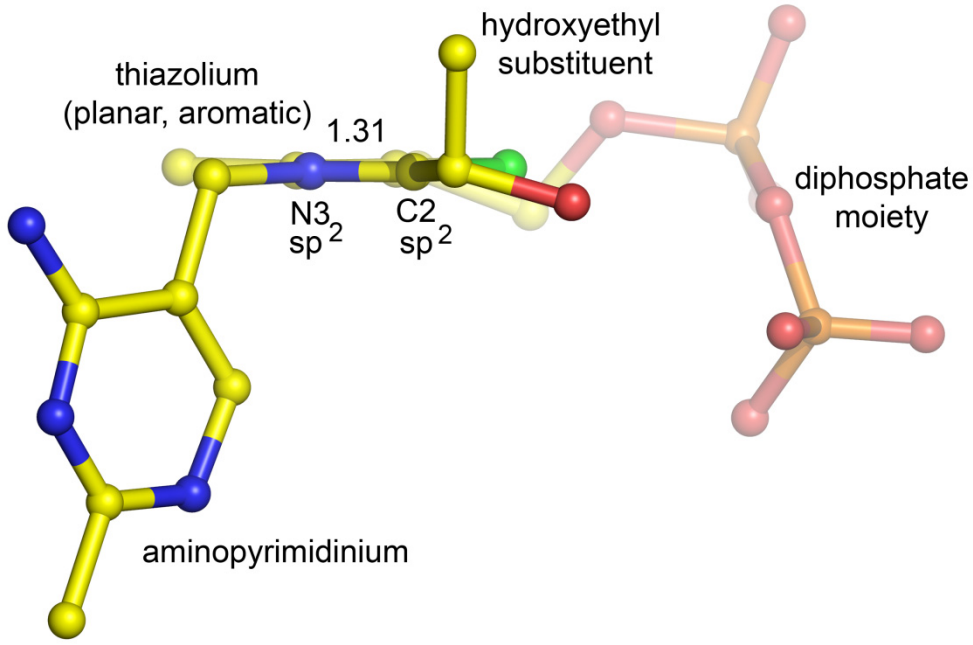

SI Fig. 4. Crystal structure of nonenzymic 2α-hydroxyethyl-thiamin diphosphate (Cambridge database code LWIREO) highlighting the aromatic nature of the C2-substituted thiazolium (2). The hybridization states of atoms C2 and N3 as well as their interatomic distance are indicated. Note the difference between this small molecule structure and the nonaromatic carbanion-enamine species trapped in pyruvate oxidase with a distorted thiazolium (see paper).

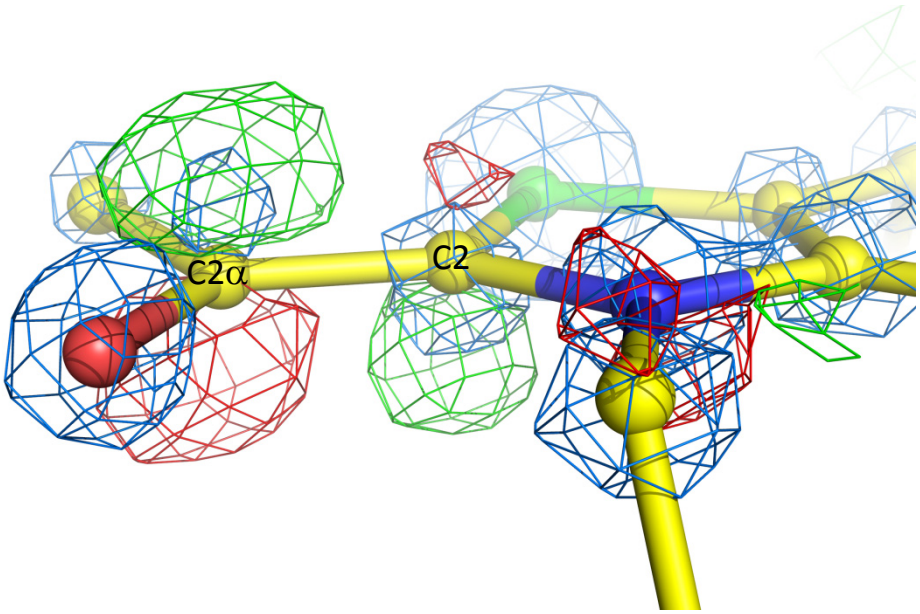

SI Fig. 5. Structure of the carbanion-enamine in POX obtained after refinement using tight in-plane restraints for the thiazolium heterocycle and the substrate atoms, which enforced a planar enamine-type structure (**3b** in Fig. 3). Please note that the derived electron density of the intermediate cannot be explained by the presence of an enamine as indicated by the pronounced positive (green, contour level 3σ) and negative (red, contour level -3σ) difference electron density peaks around atoms C2 and C2α. The corresponding 2mFo-DFc map (blue) is shown at a contour level of 3σ.

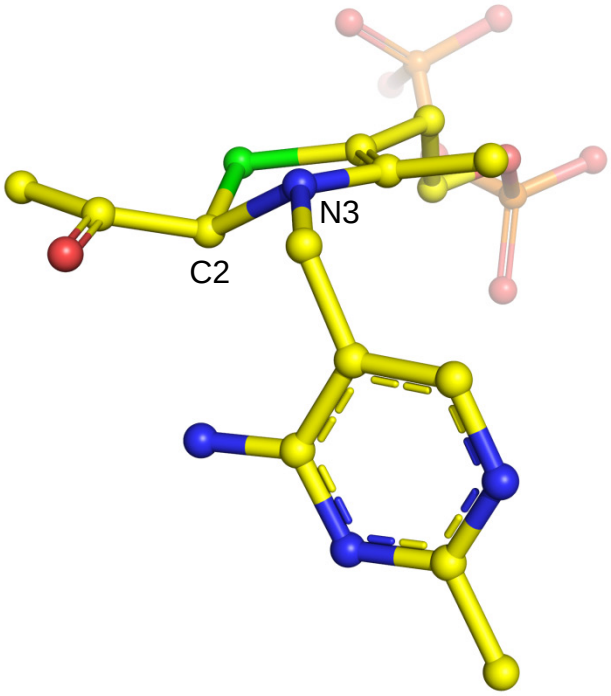

SI Fig. 6. Structure of (2*R*, 3*S*)-2-acetyl-thiazoline-ThDP. Note that atoms C2 and N3 are stereocenters (N3 is a lone-pair stereocenter). Preferential stabilization of the (3*S*)-stereo-isomer on the enzyme would result in a distorted thiazolium ring with C2 being out of plane as observed in the structure of POX (see Fig. 2).

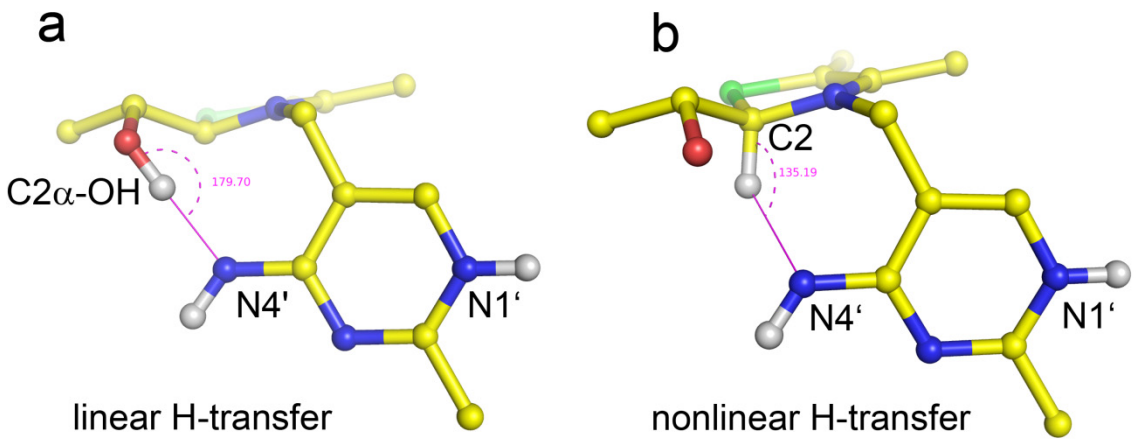

SI Fig. 7. Structure of the hydroxyethyl-ThDP carbanion-enamine intermediate trapped in POX highlighting the angles between atoms C2α-O–H–N4' (**a**) and C2–H–N4' (**b**). Note that a potential proton transfer between C2α-O and imino-N4' would have almost perfect linear geometry, whereas transfer between imino-N4' and C2 would have nonlinear geometry (deviation of ~45° from linearity), and would thus be unfavorable. Hydrogens at riding positions have been added for atoms N4', N1', C2 and C2α-O.

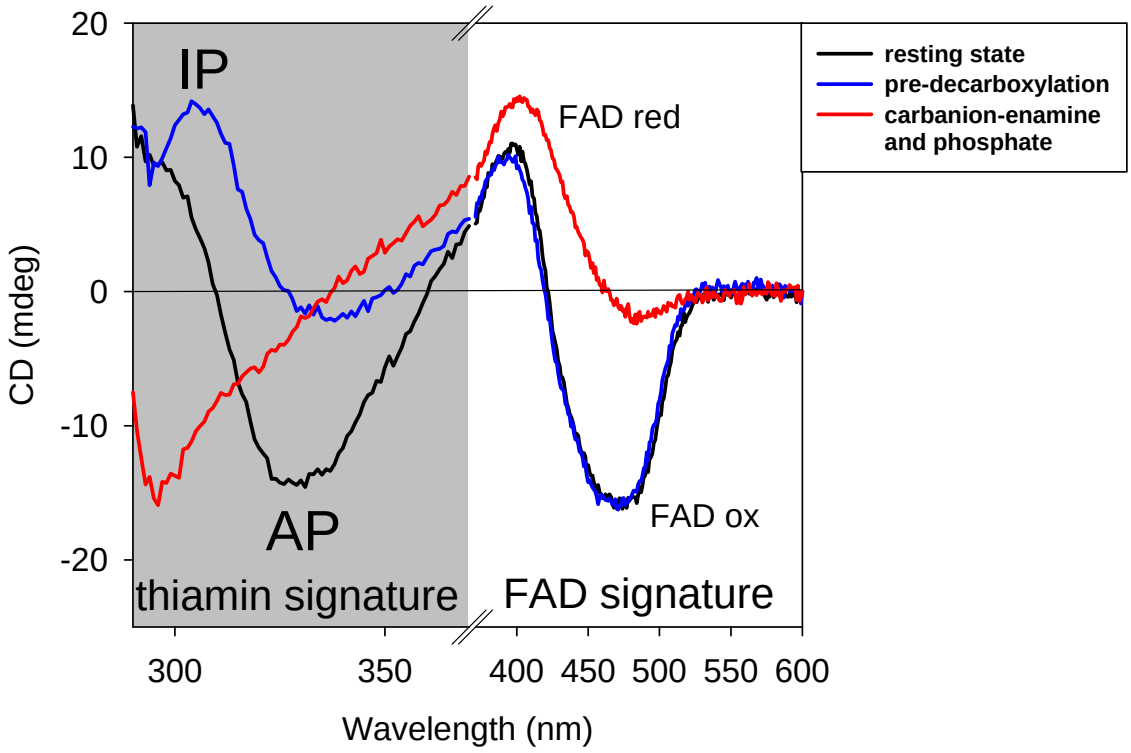

SI Fig. 8. CD spectroscopic analysis of tautomeric and ionization states of the ThDP aminopyrimidine (see Fig. 1b) at different catalytic stages in POX: i) resting state (black line), ii) pre-decarboxylation state (blue line, generated upon adding saturating amounts of substrate analog methyl acetylphosphonate) and iii) carbanion-enamine in the presence of phosphate (red line, formed after reaction with substrate pyruvate for 30 s). Note that POX predominantly stabilizes the AP form (negative signal centered around 330 nm) at the resting state (in equilibrium with IP), and the IP form (positive signal centered around 300 nm) at the pre-decarboxylation state. Neither form is accumulated at the carbanion-enamine state prompting us to conclude that the APH^+ form is mainly stabilized. The APH^+ species is expected to exhibit a CD band below 300 nm, which, owing to the high protein concentrations, cannot be resolved spectroscopically. Species were assigned according to *ref* (3).

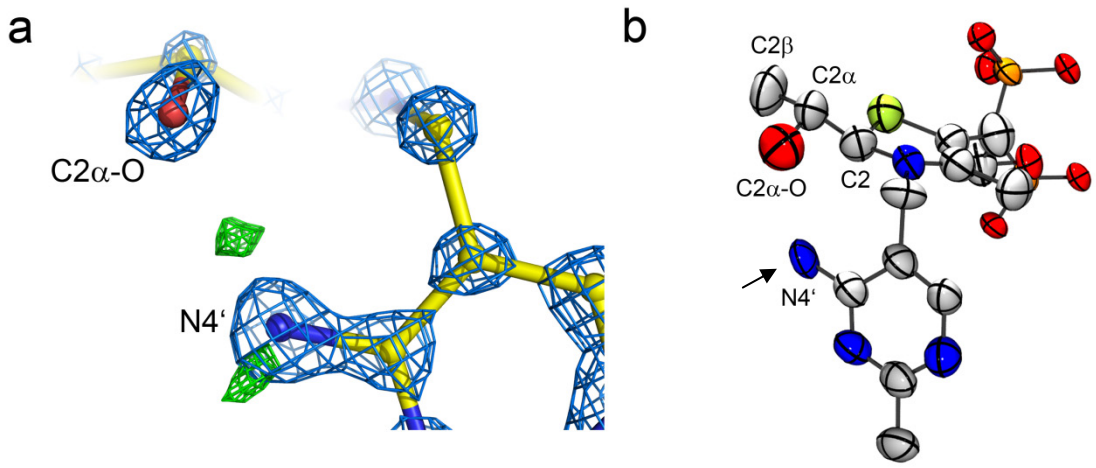

SI Fig. 9. Analysis of the protonation state of the cofactor aminopyrimidine and of the atomic displacement parameters. (**a**) The final refined model of the carbanion-enamine and the corresponding 2Fo-Fc electron density map (blue) contoured at 4σ are shown. In addition, the σ_A-weighted Fo-Fc difference electron density map (green) around atom N4‘ is shown (contour level 3σ, carved 1.5 Å around N4‘) suggesting N4‘ to be in linkage with two hydrogens as evidenced by the pronounced positive difference density peaks at the expected riding positions (Crystal B, subunit A). (**b**) Ortep plot (50% probability) showing the anisotropic displacement parameters for the carbanion-enamine intermediate (Crystal B, subunit A). Note that the principal axis for displacement of N4‘ is directed towards C2α-O supporting our proposal of a reversible internal proton transfer between C2α-O and N4‘. Software ORTEP-3 was used to generate SI Fig. 9b (4).

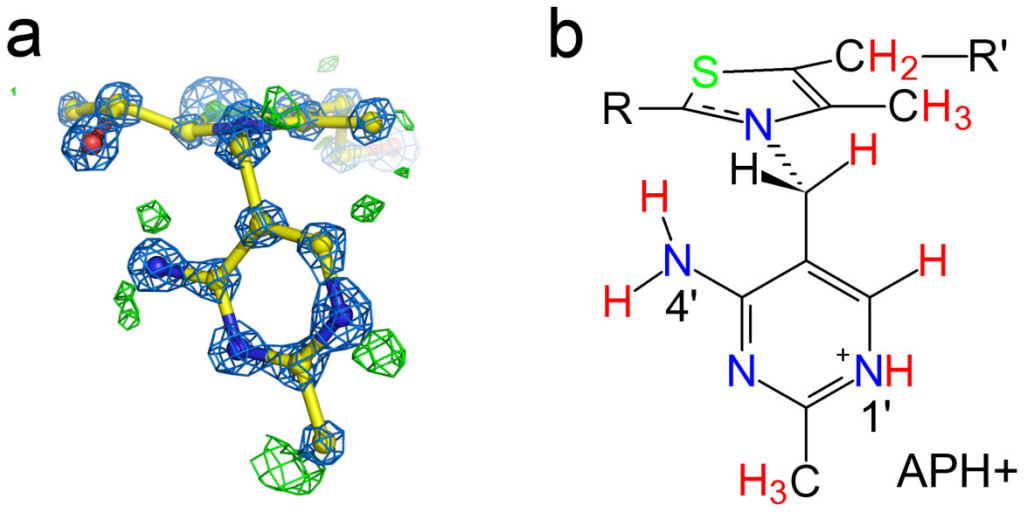

SI Fig. 10. Complete assignment of the protonation state of the carbanion-enamine in POX in one active site (crystal A, subunit A). (**a**) The final refined model, the corresponding 2Fo-Fc electron density map (blue, contour level 4σ) and the σ_A-weighted Fo-Fc difference electron density map (green, contour level 2.8σ, carved 1.5 Å around the intermediate) are shown. Positive peaks in the difference density map are only observed for expected hydrogen riding positions. Detected and assigned hydrogens are highlighted in red color in (**b**). Note that no hydrogens are detectable for the substrate-derived atoms consistent with our proposal of an equilibrium between a hydroxyethyl and an acetyl (ketone) species. The protonation state of the carbanion-enamine in the other active sites cannot be assigned unambiguously as the difference electron density around the intermediate is more diffuse.

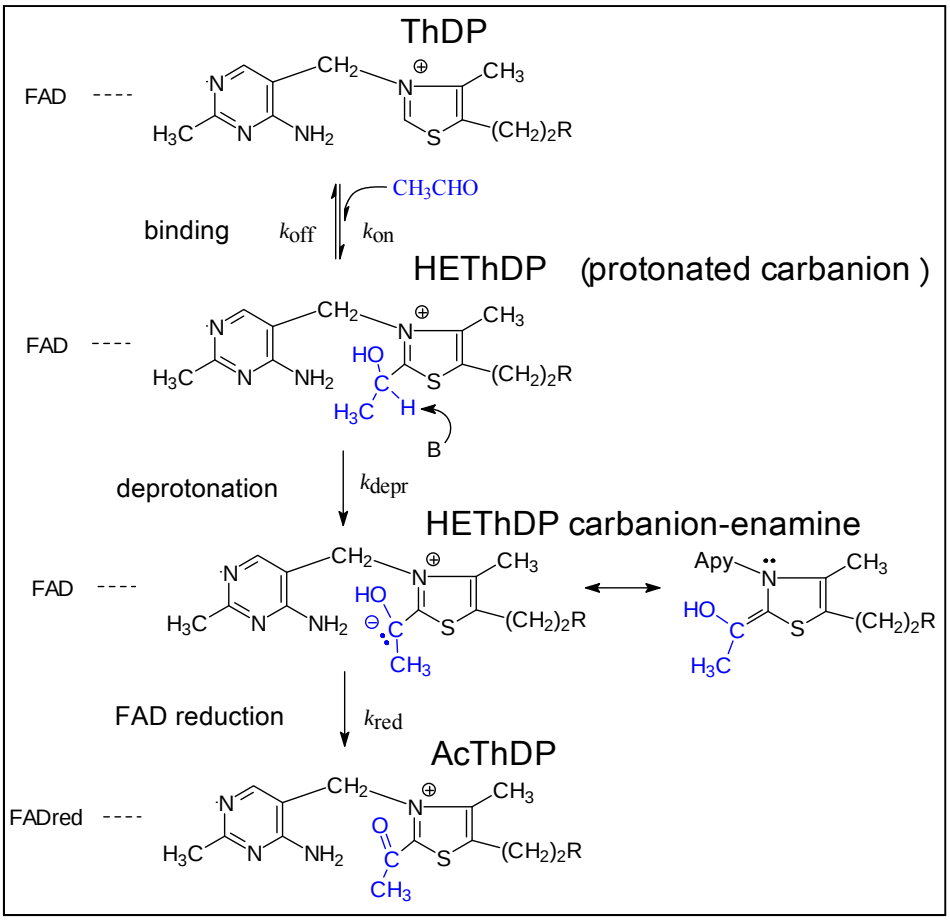

SI Scheme 1. Reductive half-reaction of POX and artificial substrate acetaldehyde with intermediates and microscopic rate constants identified. Note that prior to FAD reduction, the initially formed HEThDP (**3g** in Fig. 3, conjugate acid of carbanion-enamine with protonated C2α) must be deprotonated.

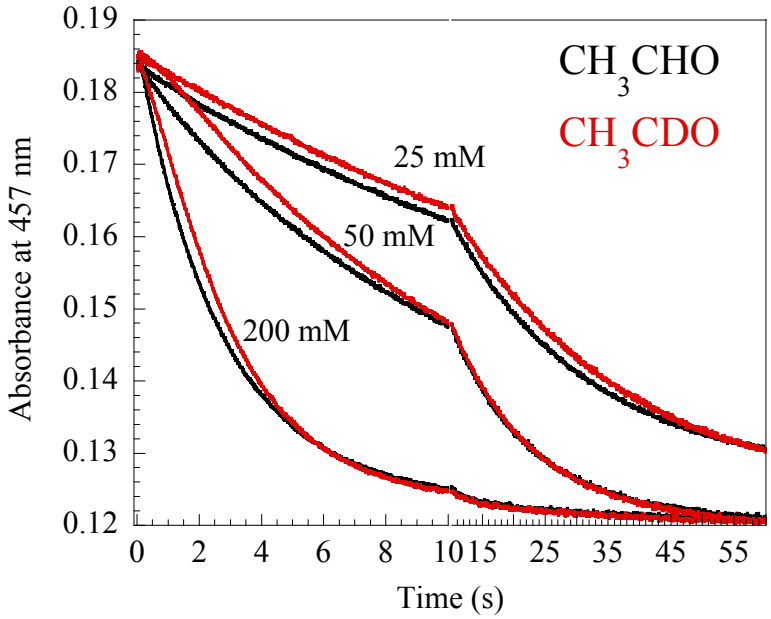

SI Fig. 11. Reductive half-reaction of POX with artificial substrate acetaldehyde (black lines) and a *d*-isotopolog of acetaldehyde (red lines) bearing a deuterium (D, ^{2}H) instead of protium at C1. Microscopic rate constants of turnover were estimated by global fit analysis using program Dynafit (see SI Scheme 1 and SI Table 2) (5).

	k_{on} (M^{-1} s^{-1})	k_{off} (s^{-1})	k_{depr} (s^{-1})	k_{red} (fixed)
acetaldehyde	3.8 ± 0.2	6.6 ± 0.2	**10.8 ± 1.4**	422
d-acetaldehyde	2.8 ± 0.3	3.8 ± 0.5	**1.9 ± 0.2**	422

SI Table 2. Microscopic rate constants for POX-catalyzed turnover of artificial substrate acetaldehyde as calculated by global fit analysis using DYNAFIT (3). As expected, we observe a large primary kinetic isotope effect (~5.7) for deprotonation of the transiently formed HEThDP intermediate. The estimated rate constant for deprotonation of HEThDP (k ~10 s^{-1}) to give the carbanion-enamine is approx. one order of magnitude smaller than k_{obs} (~80 s^{-1}) estimated for re-establishment of the steady state (see SI Fig. 12). We thus conclude that the HEThDP intermediate (**3g**, protonated carbanion-enamine) is kinetically not competent to account for the observed reactivity of the "authentic" carbanion-enamine intermediate that is accumulated on the enzyme after incubation with native substrate pyruvate.

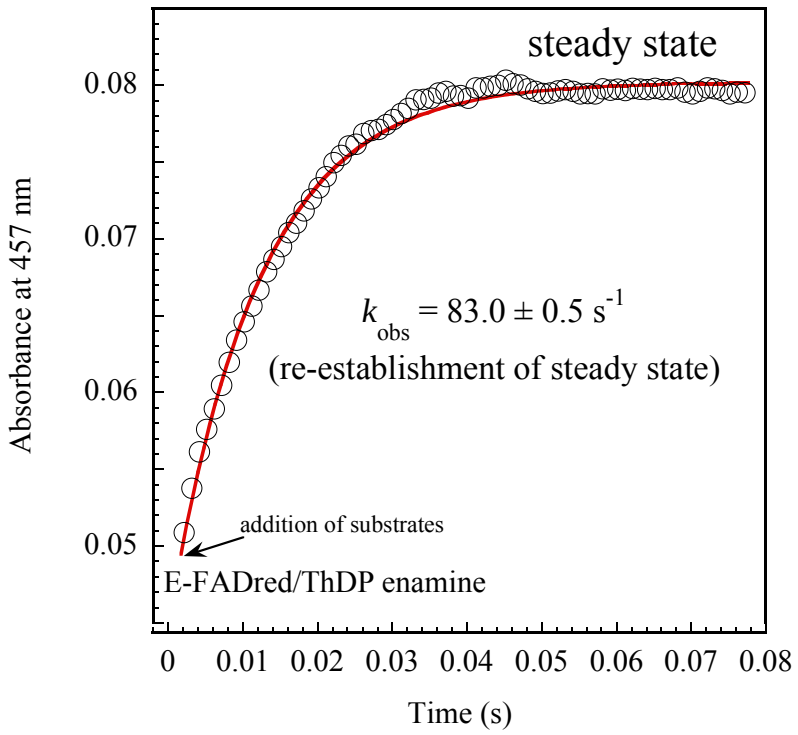

SI Fig. 12. Time-course of reaction of POX containing the HEThDP carbanion-enamine and two-electron reduced FAD (generated by pre-incubation of POX with all substrates until complete consumption of oxygen) with substrates pyruvate, oxygen and phosphate monitored at 457 nm (intrinsic FAD absorbance). Addition of substrates to the enzyme leads to re-establishment of the steady state with k_{obs} = 83.0 ± 0.5 s^{-1}. If POX was to accumulate the conjugate acid of the carbanion-enamine with protonated C2α (HEThDP), one would expect a longer pre-steady state and a k_{obs} of ~10 s^{-1} (see SI Fig. 11).

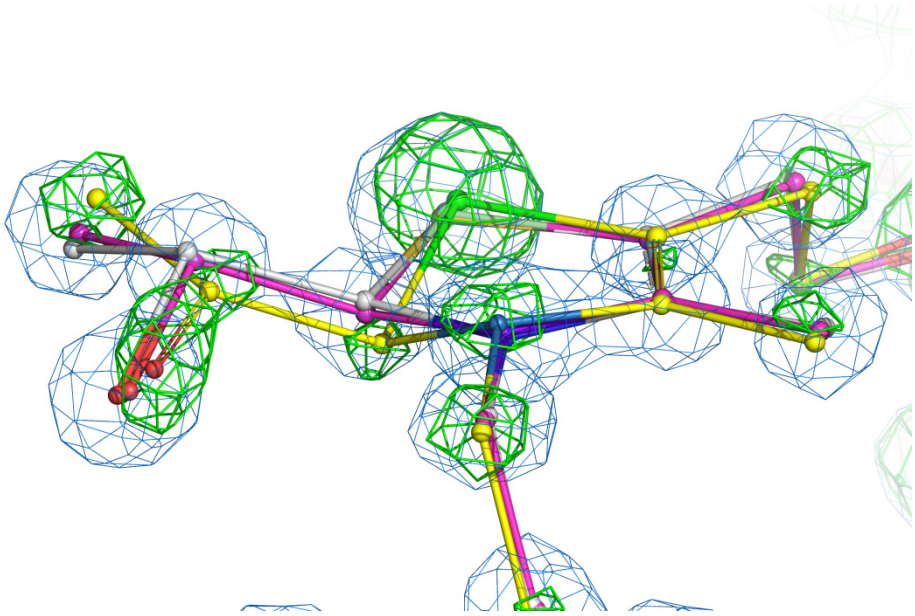

SI Fig. 13. Structures of the presumed tautomeric carbanion-enamine forms in POX. The final refined models of the two tautomeric forms (grey: aromatic species with tetrahedral C2α, yellow: nonaromatic ketone with planar C2α) are shown in ball-and-stick representation with the corresponding 2mFo-DFc electron density map (blue, contoured at 3σ). The fitted occupancies amount to 70% (aromatic form: alkoxide **3f**/carbanion **3a**) and 30% (nonaromatic ketone **3d**/**3e**), respectively. If only the aromatic species is considered in the model, positive difference electron density (green, contoured at 6σ) is observed for the ketone species. The bonding around atom C2α of the presumed ketone form is planar and the fitted bond length of the C2α-O bond is 1.23 Å, which is typical for a double bond. The weighted average of both forms as obtained by fully unrestrained refinement of all atoms and considering only one chemical species is shown in magenta. Refinements were carried out with a pre-release version of Shelx-2011.

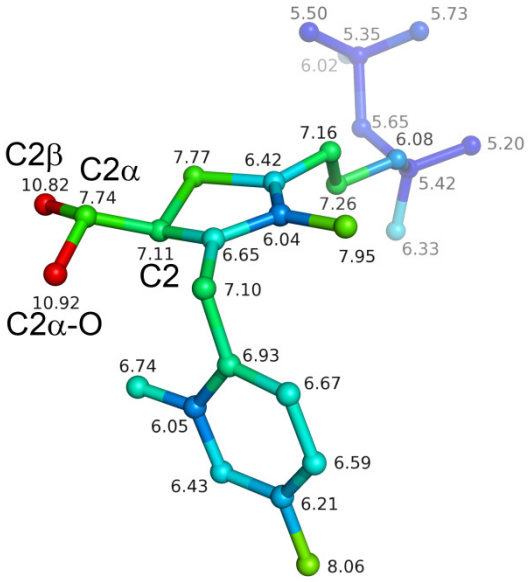

SI Fig. 14. Structure of the carbanion-enamine intermediate in POX showing the individual *B*-factors of all atoms. Note that the highest *B*-factors are observed for the substrate atoms consistent with our proposal of an interconversion between a hydroxyethyl and ketone functionality. Atoms are color-coded according to their individual *B*-factors in "blue-green-red" style showing less mobile atoms in blue (5 $Å^2$) and most mobile ones in red (11 $Å^2$).

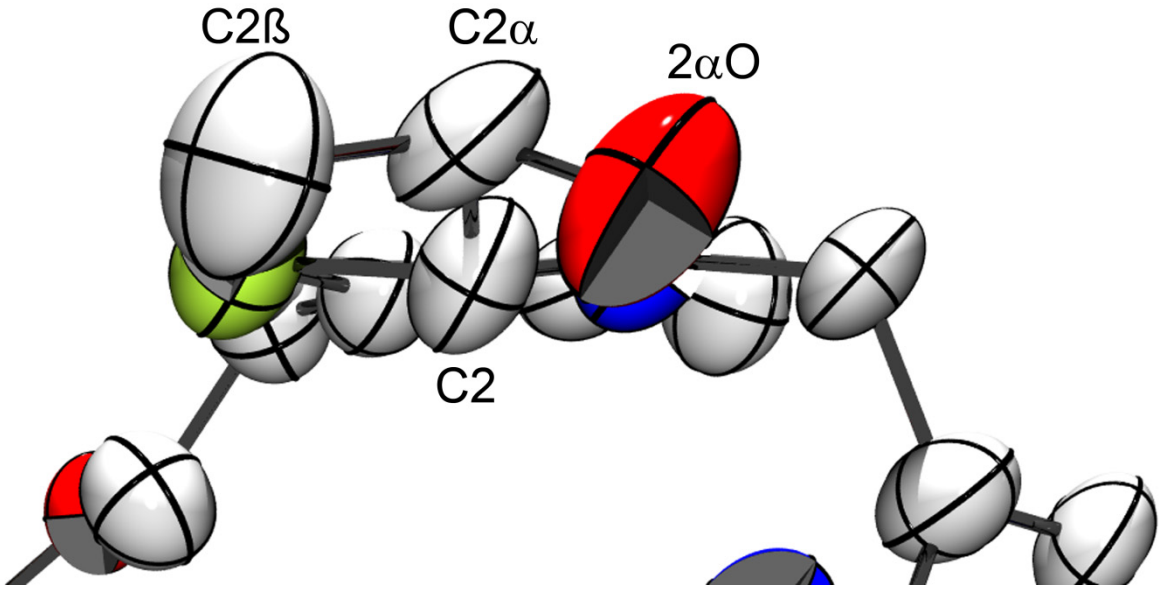

SI Fig. 15. Ortep plot (50% probability) showing the anisotropic displacement parameters for the carbanion-enamine intermediate in POX. The thermal ellipsoids of substrate-derived atoms C2α, C2ß and 2αO are - due to their incoherent orientations - not consistent with a rigid-bond criterion (anisotropic displacement components of two atoms along the bond joining them should be equal!) (6, 7). Our observation thus strongly suggests that the ellipsoids represent atomic displacements in response to chemical changes (space average of 2 species) rather than intrinsic thermal motions of one discrete species. The fitted ellipsoids are consistent with our proposed interconversion between a hydroxyethyl (C2α-O single bond) and ketone (C2α=O double bond) moiety and the implicit change of bond order of the C2α-O bond.

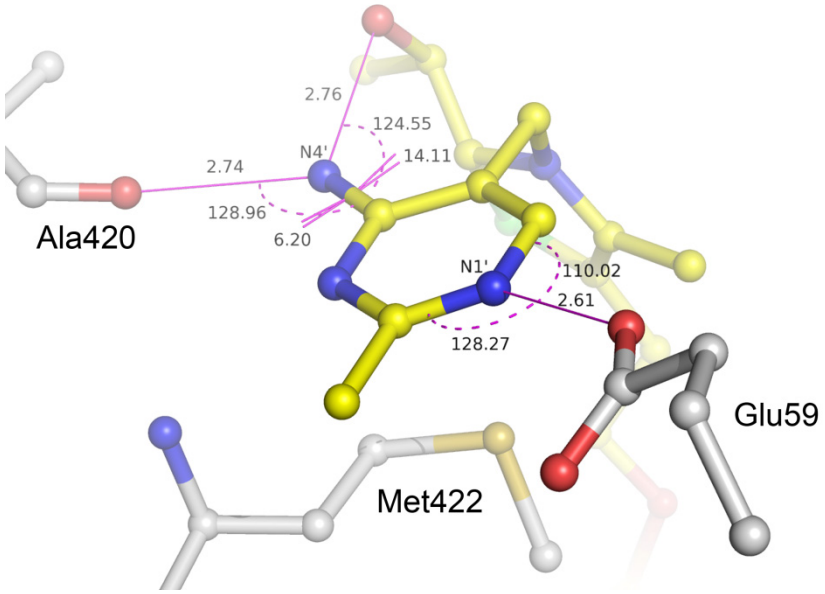

SI Fig. 16. Local interactions of the aminopyrimidine part of the carbanion-enamine in POX. Selected bond-lengths, angles and dihedrals are indicated. Note that the H-bond vectors for interactions of N4' with the backbone carbonyl of Ala420 (~6°) and C2α-O (~14°) are slightly out of the aromatic ring plane of the aminopyrimidine.

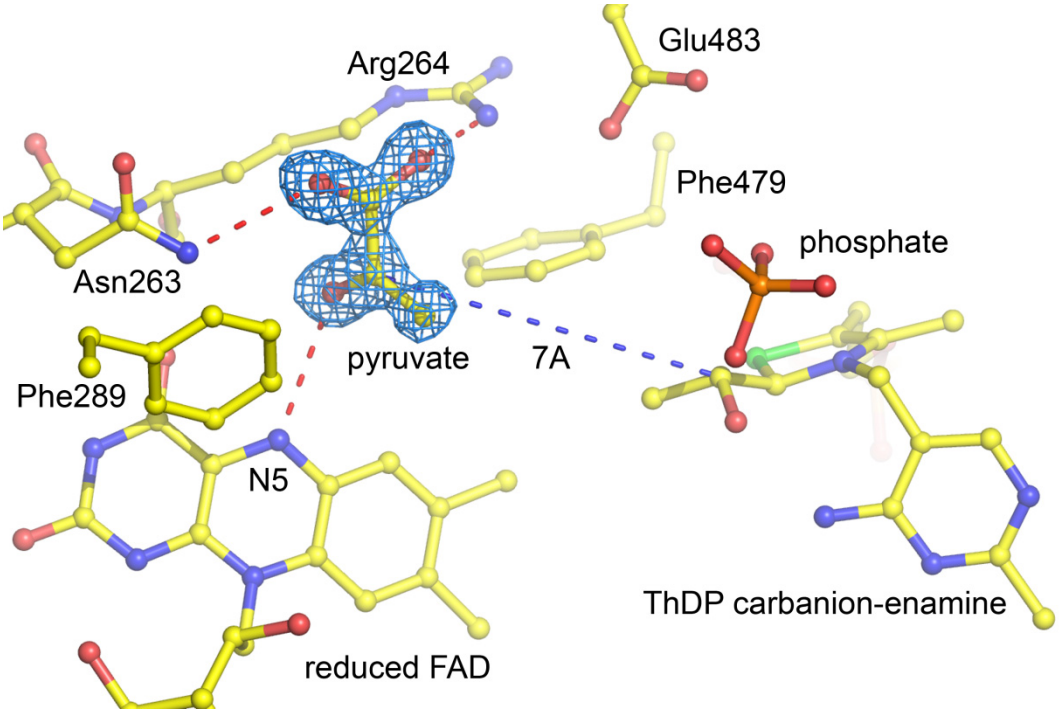

SI Fig. 17. Active site of POX showing the ThDP carbanion-enamine, two-electron reduced FAD, substrate phosphate, selected amino acid residues and electron density (blue, 1.8σ contour level) assigned to originate from bound substrate pyruvate. Hydrogen-bonding interactions of pyruvate with N5 of two-electron reduced FAD, and with side chains Asn263 and Arg264 are indicated.

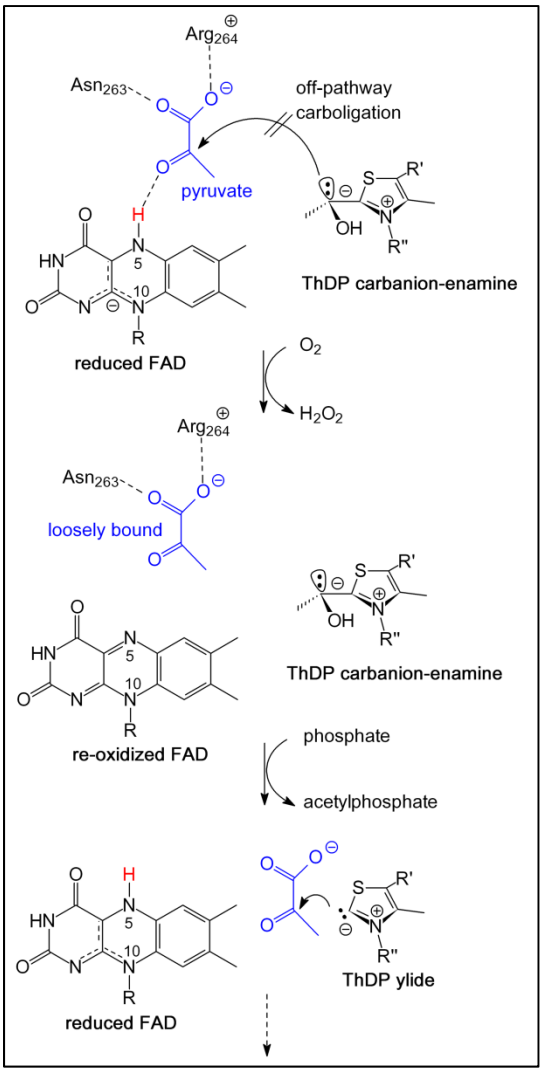

SI Fig. 18. Proposed "redox-sensing" mechanism of substrate binding in POX, according to which pyruvate binds to a docking site close to FAD and forms specific H-bonds with N5-H of two-electron reduced FAD and residues Asn263/Arg264. Such binding slightly remote from the carbanion-enamine will prevent/minimize off-pathway carboligation of the latter with pyruvate (acetolactate as product as catalyzed by the related acetohydroxyacid synthases), and rather allow substrate phosphate to attack. Reoxidation of FAD by oxygen is likely to loosen the interaction of pyruvate allowing it to react with ThDP. Note that this binding mode is likely to be only relevant for the reduced enzyme.

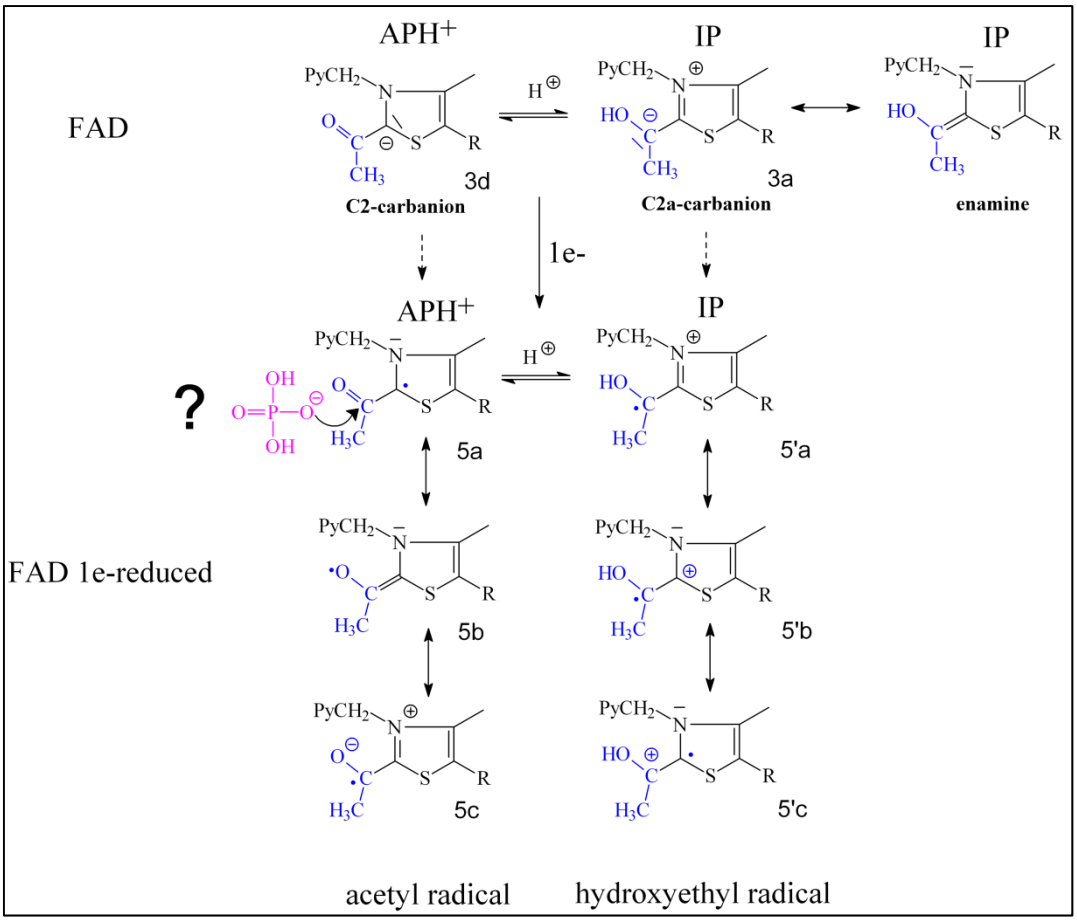

SI Fig. 19. Proposed mechanism of redox coupled acyl transfer to phosphate in POX. Note that internal proton transfer between the substrate-derived hydroxyethyl moiety and the cofactor aminopyrimidine drives reversible ketonization of the carbanion-enamine and (presumably) also of the subsequently formed ThDP radical. While ketonization is of no obvious catalytic advantage for initial one-electron reduction of FAD, it might facilitate attack of substrate phosphate at the free radical state. Of the many imaginable acetyl and hydroxyethyl radical contributors, acetyl radical species **5a** seems to be appropriate in terms of reactivity (low local charge at C2α: electrophilic center) and stability. In fact, the X-ray structure of the free ThDP radical in the related pyruvate:ferredoxin oxidoreductase suggested accumulation of **5a** on this enzyme (8). Note that hydroxyethyl radical **5'c** with a C2α-centered carbocation would also exhibit a low local charge at C2α and might potentially react with phosphate. It is questionnable, however, whether such high-energy species could be stabilized on the enzyme.

References SI Tables, Figures and Schemes

1. Tittmann K (2009) Reaction mechanisms of thiamin diphosphate enzymes: redox reactions. *FEBS J* 276:2454-2468.
2. Malandrinos G, *et al.* (1998) On the mechanism of action of thiamin enzymes, Crystal structure of 2-(α-hydroxyethyl)thiamin pyrophosphate (HETPP). Complexes of HETPP with zinc(II) and cadmium(II). *J Biol Inorg Chem* 3: 437-448.
3. Nemeria N, *et al.* (2007) The 1',4'-iminopyrimidine tautomer of thiamin diphosphate is poised for catalysis in asymmetric active centers on enzymes. *Proc Natl Acad Sci USA* 104:78-82.
4. Farrugia LJ (1997) ORTEP-3 for Windows - a version of ORTEP-III with a Graphical User Interface (GUI) *J Appl Cryst* 30: 565.
5. Kuzmic P (1996) Program DYNAFIT for the analysis of enzyme kinetic data: application to HIV proteinase. *Anal Biochem* 237: 260-273.
6. Hirshfeld FL (1976) Can X-ray Data Distinguish Bonding Effects from Vibrational Smearing? *Acta Cryst* A32: 239-244.
7. Thorn A, Dittrich B, Sheldrick GM (2012) Enhanced rigid-bond restraints. *Acta Crystallogr Sect A* 68: in press.
8. Chabriere E, *et al.* (2001) Crystal structure of the free radical intermediate of pyruvate:ferredoxin oxidoreductase. *Science* 294: 2559-2563.